Substoichiometric cobalt oxide monolayer on Ir(100)-(1 × 1)

2009 J. Phys.: Condens. Matter 21 474211

(http://iopscience.iop.org/0953-8984/21/47/474211)

J. Phys.: Condens. Matter **21** (2009) 474211 (7pp) doi:10.1088/0953-8984/21/47/474211

Substoichiometric cobalt oxide monolayer on Ir(100)-(1 × 1)

M Gubo, C Ebensperger, W Meyer, L Hammer and K Heinz

Lehrstuhl für Festkörperphysik, Universität Erlangen-Nürnberg, Staudtstraße 7, D-91058 Erlangen, Germany

E-mail: klaus.heinz@physik.uni-erlangen.de

Received 2 April 2009, in final form 29 April 2009
Published 5 November 2009
Online at stacks.iop.org/JPhysCM/21/474211

Abstract

A substoichiometric monolayer of cobalt oxide has been prepared by deposition and oxidation of slightly less than one monolayer of cobalt on the unreconstructed surface of Ir(100). The ultrathin film was investigated by scanning tunnelling microscopy (STM) and quantitative low-energy electron diffraction (LEED). The cobalt species of the film reside in or near hollow positions of the substrate with, however, unoccupied sites (vacancies) in a 3 × 3 arrangement. In the so-formed 3 × 3 supercell the oxide's oxygen species are both threefold and fourfold coordinated to cobalt, forming pyramids with a triangular and square cobalt basis, respectively. These pyramids are the building blocks of the oxide. Due to the reduced coordination as compared to the sixfold one in the bulk of rock-salt-type CoO, the Co–O bond lengths are smaller than in the latter. For the threefold coordination they compare very well with the bond length in oxygen terminated CoO(111) films investigated recently. The substoichiometric 3 × 3 oxide monolayer phase transforms to a stoichiometric c(10 × 2)-periodic oxide monolayer under oxygen exposure, in which, however, cobalt and oxygen species are in (111) orientation and so form a CoO(111) layer.

(Some figures in this article are in colour only in the electronic version)

1. Introduction

Today ultrathin oxide films of transition metals play an important role in basic research as well as in applications for magneto-electronic devices. For larger film thicknesses they appear in many cases in the stoichiometry and structure of the bulk material. Then they are in most cases antiferromagnetic (AFM); i.e., when contacted with the ferromagnetic (FM) phase of the transition metal they exhibit the phenomenon of exchange bias [1, 2], which is of considerable influence with respect to the magnetism of nanosized AFM/FM systems. For cobalt oxide grown on Ir(100) as a support we have extensively studied the structure and morphology for thicker films recently. They have been shown to be non-pseudomorphic and of (111) orientation, being of spinel-type Co_3O_4 structure when prepared under oxygen rich conditions [3] and of rock-salt-type CoO structure when the spinel-type films lose a quarter of their oxygen content by thermal annealing [4]. Interestingly, the rock-salt-type films exhibit an anomalous wurtzite-type stacking near the surface [5] and form a ($\sqrt{3}$ × $\sqrt{3}$)R30° superstructure in their low-temperature ground state [6].

With further miniaturization of devices, i.e. with decreasing thicknesses of the films involved, both the structure and stoichiometry of the oxide films as well as their magnetic properties may substantially deviate from those of thicker films. In this light we present a structural investigation of the thinnest possible film, which consists of only a single monolayer (ML) of cobalt oxide, whereby again the unreconstructed surface of Ir(100) is used as a support. We regard this geometric structure as interesting and important due to the well known intimate relationship between structure and magnetism, even though the latter is not investigated in the present work.

The paper is organized as follows. In section 2 we describe the preparation of films. This is followed by a section introducing the methods applied, namely low-energy electron diffraction (LEED) including the structural analysis of intensities and scanning tunnelling microscopy (STM). Subsequently, the results are presented and then discussed in section 4.

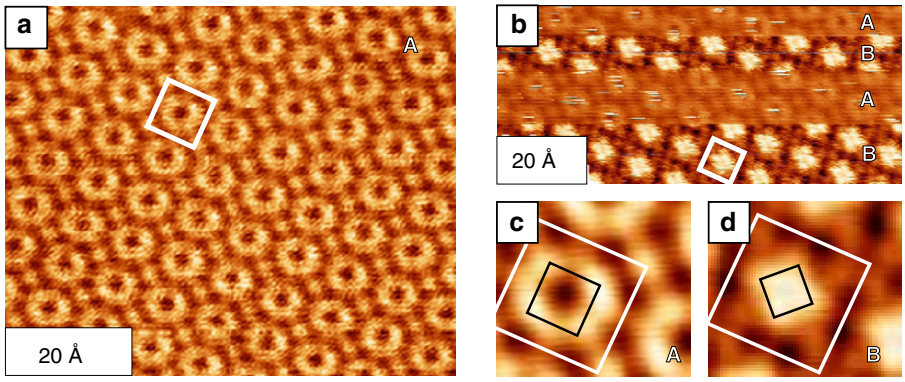

Figure 1. Appearance of the 3 × 3 superstructure at a tip voltage of $U = 23$ mV ($I = 3.2$ nA) in panels (a) and (c). In panel (b) the tip voltage is switched twice from 23 to 2 mV ($I = 9.5$ nA each), so that stripes of different appearances develop, namely of type A (as in panel (a)) and of type B. Panels (c) and (d) result from averages over many 3 × 3 unit cells (given by white lines) with appearances of type A and B respectively. The intensities are at a maximum at the corners of the squares inserted as black lines.

2. Experimental and computational details

In thermodynamic equilibrium the Ir(100) surface exhibits a (5 × 1) superstructure [7, 8] denoted as Ir(100)-(5 × 1)-hex. A clean and unreconstructed Ir(100)-(1 × 1) phase results by reconstruction-lifting adsorption of oxygen followed by the removal of oxygen by exposure to hydrogen [9–11]. Though this clean surface is metastable it can be used as support for the oxide film as it is stabilized by adsorbates. The sample was mounted in a two-stage ultra-high vacuum (UHV) apparatus with one of the two vessels hosting a homemade three-grid LEED optics and an electron-beam operated evaporator for highly purified cobalt. The second vessel, to which there was easy sample transfer without breaking the UHV, was provided with a commercial beetle-type STM (RHK Instruments).

The cobalt oxide film was prepared by deposition of slightly less than 1 ML cobalt at a deposition rate of about 1 ML min^{-1} with the substrate held at 50 °C (note that 1 ML Co corresponds to a coverage of 1.36×10^{15} cm^{-2} on Ir(100)-(1 × 1)). Subsequently, the cobalt layer was oxidized by exposure to oxygen at a pressure of about 5×10^{-9} mbar for about 7.5 min with the sample again held at 50 °C. By this procedure the appearing 3 × 3 superstructure was developed best. Loss of oxygen by annealing was monitored by thermal desorption spectroscopy (TDS) as described earlier [4, 11].

STM images were taken for the sample at room temperature, whereby atomic resolution could be achieved with tip voltages in the mV range. For the image processing the program described in [12] was applied. LEED patterns and intensity versus energy spectra, $I(E)$, were recorded as input for the structural analysis. They were measured for normal incidence of the primary beam with the sample cooled to liquid nitrogen temperature. For the measurement a 12-bit digital charge-coupled-device (CCD) camera viewing the LEED screen from outside the UHV was used. The diffraction patterns were stored on a computer's hard disk in energy steps of 0.5 eV and the $I(E)$ spectra resulted by off-line evaluation of the video signal under computer control with automatic background subtraction involved [13]. Spectra of beams symmetrically equivalent at normal incidence were averaged in order to improve the signal/noise ratio. The total energy width of the data base as accumulated over 31 symmetry-inequivalent beams (7 integer order and 24 fractional order beams) amounts to as much as $\Delta E = 12\,500$ eV.

The measured spectra were analysed by application of the perturbation method TensorLEED [13–15] using the code TensErLEED [16]. For the structural search a frustrated annealing procedure [17] was used. It is controlled by the Pendry R-factor to compare experimental and computed spectra quantitatively [18]. A maximum of 14 phase shifts calculated after [19] and corrected for thermal diffuse scattering was used. Electron attenuation was simulated as usual by an optical potential, which in the course of the fit procedure was determined as $V_{0i} = 6.0$ eV. The real part of the inner potential was taken as energy dependent according to [19] in order to account for the energy dependence of the exchange–correlation potential. In initial test calculations possible vacancies were considered on the basis of the average T-matrix approximation (ATA) [20] used in the version of chemical TensorLEED [13, 21, 22] also implemented in the TensErLEED program package.

3. Results

3.1. STM images

In figure 1 STM images of the 3 × 3 superstructure are displayed. The image in panel (a) was recorded by a positive tunnelling tip with $U = 23$ mV and a current of 3.2 nA. Evidently, atomic resolution is achieved. At each corner of the 3 × 3 unit cell, which is inserted in the image, a single protrusion shows up, which possibly can be interpreted as an atomic image. As the other features are a bit more fuzzy we averaged the STM signal over many unit cells with the average given in panel (c). As a result four more atomic features in quadratic arrangement within the unit cell appear.

Surprisingly, the appearance of the STM image is considerably modified by only a small change of the tip voltage. Figure 1(b) shows four horizontal image stripes between which the tip voltage was changed. The upper stripe

was recorded at the same voltage as used in panel (a) and so displays the same image characteristics (denoted by A). For the second stripe the voltage was changed to $U = 2$ mV and a new appearance of the image (denoted by B) develops. Further switches of the voltage make features A and B reappear as indicated. Averaging the image of type B over many unit cells produces again a quadratic arrangement of bright image intensities within the unit cell. However, as displayed in panel (d) they are—in contrast to images of type A—rotated by 45° with respect to the unit mesh square. Additionally, there are four more protrusions around the corners of the unit cell, but with much lower intensities.

3.2. LEED intensity analysis

Even if we assume the bright image maxima in panels (c) and (d) of figure 1 to be atomic images, we cannot easily conclude a structural model, as we know neither the chemical identity of these atoms nor their geometric distance from the tip. However, without the input of a structural model—whose numerical parameter values are then determined in the course of the analysis—no structure determination in the usual way is possible. Certainly, contributions to the superstructure spot intensities can come from the arrangement of both cobalt and oxygen species, and possibly also from the substrate when the oxide layer induces it to restructure. In order to reduce the complexity of the problem we took advantage of the considerably different scattering strength of the chemical species involved and—in a first step of the intensity analysis—neglected scattering from oxygen completely. As we knew that less than 1 ML of cobalt had been deposited on the surface and with the knowledge from STM that there are no uncovered substrate patches, we allowed in preliminary test calculations for a fractional occupation of Co adsorption sites using chemical TensorLEED in a 3×3 supercell. Due to applying 4 mm symmetry there are only three groups of Co species allowing for an independent occupation number of sites, namely two groups each made up by four equivalent sites and one with only a single site. Only for the latter the fit procedure, which also allowed for vertical relaxations, led to an occupation number of less than 20% whilst it was larger than 80% for the other sites. This finding is also in line with the fact that the cobalt coverage is only slightly below 1 ML. As a consequence, we assumed for further calculations a cobalt layer with ordered vacancies in 3×3 arrangement and full occupation of the remaining sites, whereby species neighbouring vacancies were also allowed to relax laterally as displayed in figure 2(a). The structure found for this preliminary model yields R-factors of $R = 0.29$ for the spectra of integer order spots and $R = 0.43$ for those of fractional order spots. This tells us that the spacings determined for layers made up by strong scatterers (cobalt and iridium) are already close to the experimental situation, but also that—not unexpected—the scattering from the cobalt vacancies is not sufficient to fully account for the superstructure spot intensities. Nevertheless, the vacancies and the lateral relaxation seem to be an important structural element.

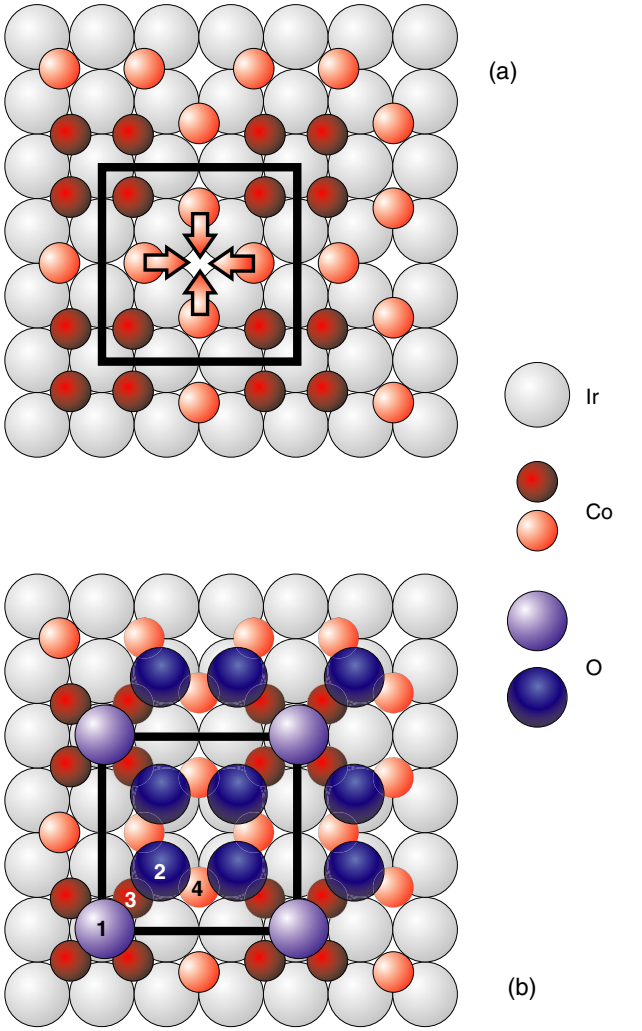

Figure 2. Model of the 3×3 superstructure for (a) the cobalt layer interfacing the oxide to the substrate and (b) the full system including the oxygen species. There are different cobalt species, those neighbouring vacancies (bright) and those which do not (dark). Also, there are oxygen species, namely in fourfold (bright) and threefold (dark) coordination to Co.

Therefore, in a second step of the analysis, we added oxygen species to the model without destroying the vacancies, whereby, of course, there are various possibilities. Eventually, a configuration fitting the experimental intensity data best was found, in which two different sites are occupied, namely with oxygen in fourfold and threefold coordination to cobalt as displayed in figure 2(b). All oxygen atoms (or ions) reside on top (or nearly on top) of iridium atoms in the substrate's top layer. There are five oxygen and eight cobalt species within the 3×3 cell. Yet, because of fourfold rotational symmetry and the presence of two mutually orthogonal mirror planes assumed, only two of each species are symmetrically inequivalent, as indicated by the numbers imprinted on the species in figure 2(b). Dependent on their location in the cell only their vertical coordinate can vary, or additionally an in-plane coordinate. This leads to a total of seven geometrical parameters for the oxide layer. Additionally, adsorbate induced modifications in the top three iridium layers were allowed,

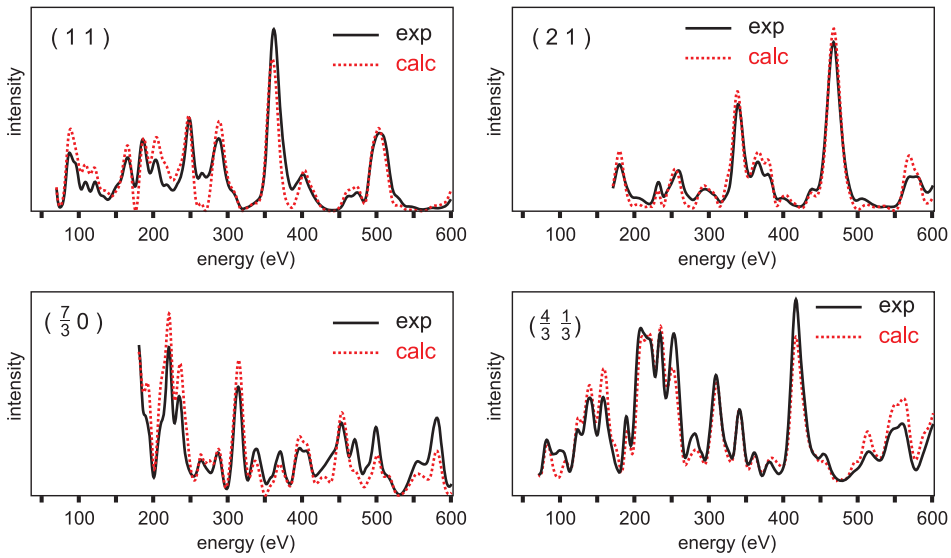

Figure 3. Comparison of experimental and best-fit model spectra for selected integer and fractional order beams.

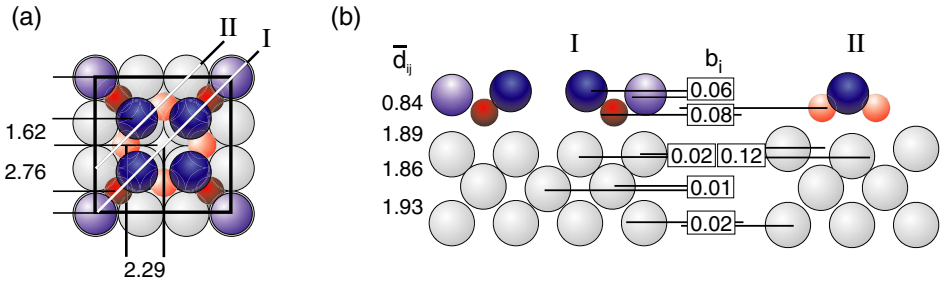

Figure 4. Best-fit model in (a) top view and (b) side views along the planes indicated by lines I and II inserted in panel (a). The best-fit structural parameters are given in ångstrøm units. For buckled layers (buckling amplitudes b_i) the interlayer spacings $\bar{d}_{ij}$ are with respect to the centre-of-mass planes. The sides of the 3×3 unit cell have a length of 8.15 Å.

which, again due to symmetry restrictions, leads to another 15 variables to be varied, so that in total the geometry of the surface is described by 22 structural parameters. In addition, the vibrations of atoms were considered. They were assumed to be isotropic, so that there is a vibrational amplitude for each of the two different oxygen species and each of the two cobalt species, whilst the amplitude of substrate atoms was fixed (0.043 Å according to a bulk Debye temperature of 420 K). So the total number of parameters to be determined amounts to 26. With the data energy width of $\Delta E = 12\,500$ eV there are $\Delta E/4V_{0i} = 521$ independent data points, so that the redundancy factor for the structure determination is as high as about 20. This means that there is no overfitting of the structural parameters by the experimental data, i.e. the fit will be on safe grounds.

The variation of the model parameters in the structural search leads to an excellent fit of model intensities to experimental data. The total R-factor is $R = 0.163$, with practically the same values holding for the subsets of integer and fractional order beams. The convincing fit quality is also mirrored by visual comparison of the spectra, as demonstrated in figure 3 for a selection of two integer and two fractional order beams.

The numerical best-fit values of the structural parameters are displayed in top and side views of the supercell in figure 4. For more clarity two side views are given, namely for the planes indicated by lines I and II in the top view panel. In the substrate, in-plane displacements were only 0.03 Å for the top layer and 0.02 Å for the second iridium layer. The buckling amplitudes in the substrate are only substantial for the top iridium layer (0.12 Å) and are within the limits of errors for deeper layers (therefore, only two examples are given in figure 4(b) and positional differences between other iridium atoms are omitted). The (isotropic) vibrational amplitudes determined amount to 0.16 Å for both oxygen species and 0.12 Å for the two cobalt species. The error limits for the parameters determined were estimated by the variance of the R-factor [18], $\mathrm{var}(R) = R_{\min}\sqrt{8V_{0i}/\Delta E} = 0.010$, whereby, however, parameter correlations were neglected. They amount to 0.02–0.03 Å for vertical parameters and 0.05–0.07 Å for in-plane parameters.

At this point we can compare the averaged STM images displayed in panels (c) and (d) of figure 1 with the structural model retrieved. Apparently, the atomic like features in panel (a) correspond to oxygen species, whilst those of panel (d) seem to be images of cobalt, whereby those cobalt species

displaced by 0.08 Å outwards with respect to the others appear much brighter than the latter. The drastic change of the unit cell appearance upon a comparatively small change of the tunnelling voltage can certainly not be due to density of state effects. We assume that it is caused by some tip–sample interaction when the tip comes very close to the surface at a voltage of only 2.0 mV and a current as high as 9.5 nA.

3.3. Transition to (111) orientation by oxygen exposure

The substoichiometric, i.e. oxygen deficient, 3 × 3 phase can be transformed to a c(10 × 2) phase by further exposure to oxygen as demonstrated in figure 5. For this transition the sample was heated to about 500 °C and then exposed to 5×10^{-8} mbar oxygen for 90 s within simultaneous lowering of the temperature to 50 °C during the exposure time. We have already observed and reported about the c(10 × 2) phase earlier [23]. For its monolayer regime a model with 1:1 stoichiometry has been proposed. This has been quantitatively confirmed in the meantime by a LEED analysis which will be published separately. Different from the 3 × 3 structure—in which cobalt and oxygen species are in square arrangement, the respective layers in the c(10 × 2) phase are of quasi-hexagonal order, i.e., the stoichiometric CoO monolayer is of (111) orientation (the hexagonal unit cell is distorted due to the film's accommodation to the square substrate [23]). The 3 × 3 phase reappears from the c(10 × 2) structure by annealing at about 800 °C, which is accompanied by some loss of oxygen as monitored by TDS. Whilst the substoichiometric phase is characterized by a mixture of three- and fourfold cobalt-coordinated oxygen the stoichiometric phase exhibits only threefold coordinated oxygen.

It is also worth noting that the 3 × 3 phase appears as well when thick CoO(111) films are annealed at temperatures in the range 700–1100 °C. Hereby the films decompose into 3D clusters with facets in between which exhibit a 3 × 3 superstructure [4] with the same diffraction intensities as in the present paper.

4. Discussion and conclusion

As evident from the final structural model displayed in figure 4, the monolayer cobalt oxide retrieved is of Co_8O_5 stoichiometry, i.e. substantially oxygen substoichiometric with respect to CoO. The spacing between the centre-of-mass planes of the cobalt and top substrate layer is at 1.89 Å much larger than the value of 1.66 Å reported for a single cobalt monolayer adsorbed on Ir(100)-(1 × 1) [24]. Taking into account that the radius of ionic cobalt is certainly smaller than that in the metal layer, this tells us that—not surprisingly—the bonding between cobalt and the substrate is considerably weakened by the formation of the oxide. This finding is also in line with the result that the interlayer spacing of the first two iridium layers (1.86 Å) is almost the same as that of the clean Ir(100)-(1 × 1) surface (1.85 Å [8]). On the other hand, the interaction of the oxide with the substrate is still strong enough to maintain a coincidence lattice with the latter. This may come by the interaction of the oxygen species with the substrate.

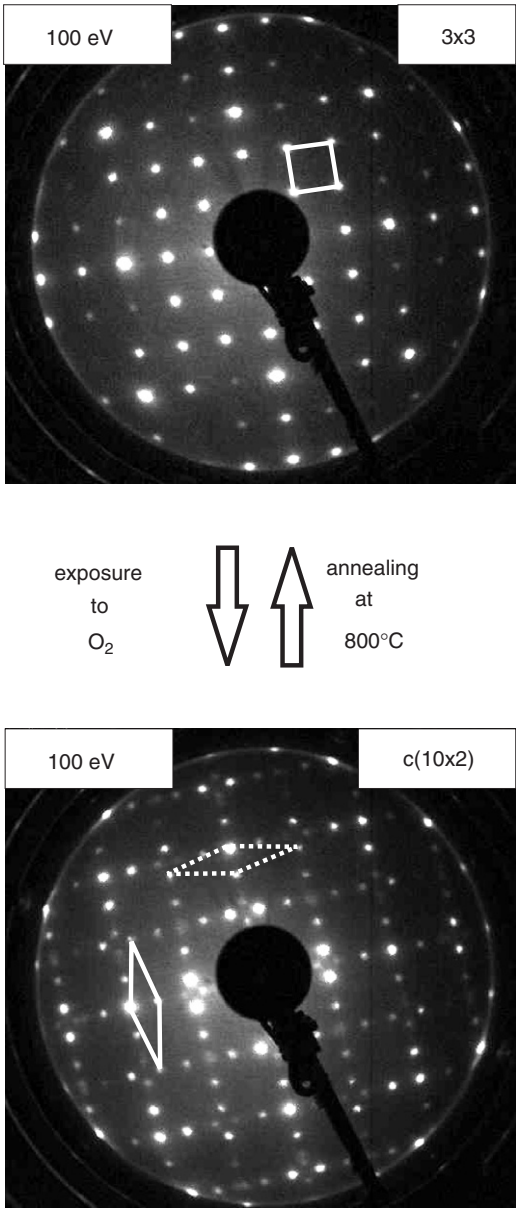

Figure 5. Top: 3 × 3 LEED pattern of the substoichiometric cobalt oxide monolayer. By exposure to additional oxygen it transforms to a c(10 × 2) superstructure (bottom panel) which has been observed already earlier [23]. By annealing, the 3 × 3 phase reappears, proving the structural transition to be reversible. The unit meshes are indicated (in the bottom panel for two orthogonal domains).

The vacancies in the cobalt layer and the corresponding substantial in-plane relaxations of the surrounding cobalt species by as much as 0.42 Å (see figure 2(a)) create threefold coordinated sites for oxygen (the angle between the undisplaced and displaced cobalt changes from 90° to about 71°). In contrast, the cobalt species around the corners of the supercell still offer fourfold coordinated sites, so that the structural elements of the oxide are pyramids with a triangle or square of cobalt species as basis and oxygen at the top of the pyramid. Four triangle-pyramids are connected to form a square arrangement within the supercell and the square-based pyramids at the corners of the supercell are the structural

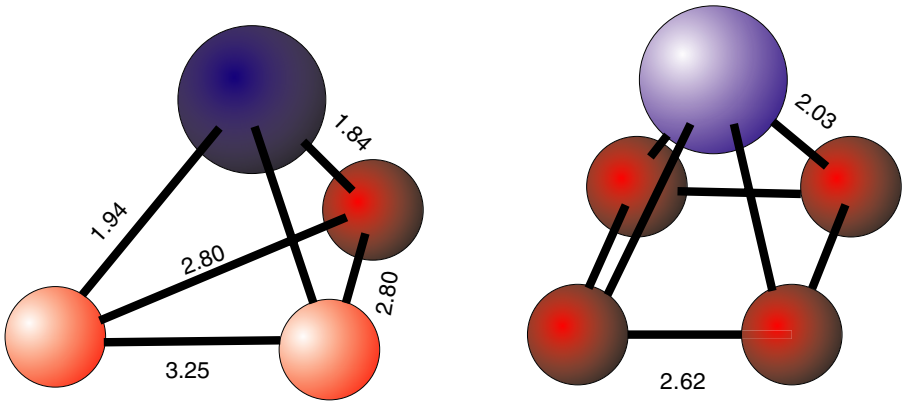

Figure 6. The two structural elements of the Co_8O_5 monolayer film: oxygen at the top of a pyramid in threefold (left) and fourfold (right) coordination to cobalt species. The bond lengths displayed are in ångstrøm units.

bridges to the neighbour cells. In figure 6 the two pyramids are displayed in perspective with the interatomic spacings inserted. In the fourfold coordinated configuration the oxygen–cobalt bond length amounts to 2.03 Å whereby in the threefold coordinated case the lengths 1.84 and 1.94 Å apply. All values are significantly smaller than the bond length in rock-salt-type CoO (2.13 Å). Yet, in view of the sixfold coordination in the CoO bulk and with the reasonable assumption that the bond length should decrease with decreasing coordination the values found for the present structure make sense. Even more, the bond lengths for threefold coordination are close to the values found recently for oxygen terminating a CoO(111) film on Ir(100), namely 1.85 and 1.86 Å [5].

The different coordination of oxygen atoms leads also to a buckling of the terminating oxygen layer by 0.06 Å and a similar one (0.08 Å) for the cobalt layer below. The buckling proceeds even to the top substrate layer. There, iridium atoms with no oxygen directly above are closer to the surface than the others by a maximum of 0.12 Å. This is consistent with the direct interaction of oxygen and iridium mentioned above. The buckling induced by the quasi-hexagonal top layer in the Ir(100)-(5 × 1)-hex phase proceeds down to the fourth layer [8]. In the present case, the buckling below the top Ir layer dies quickly away; the small values given in figure 4 are within the limits of errors as already mentioned.

As we have also shown, the substoichiometry retrieved is in line with the fact that the Co_8O_5 monolayer transforms to a stoichiometric CoO monolayer by exposure to oxygen with the reverse transition triggered by annealing (accompanied by oxygen loss). However, during the transitions not only the film's stoichiometry is changed but also its structure and crystallographic orientation, i.e. (100) ↔ (111). This is in a way surprising as for the transitions a considerable rearrangement of atoms takes place. We regard our finding to be rather important for applications with very thin oxide films involved. As structure and magnetism are intimately correlated, it is crucial to control the films' stoichiometry, structure and orientation with great care.

In conclusion, we have found a so far unreported substoichiometric cobalt oxide monolayer epitaxially grown on Ir(100)-(1 × 1). In spite of strong intraoxide bonds the oxide forms a 3 × 3 coincidence lattice with the substrate. This superstructure with respect to the substrate's unit mesh is mainly due to a 3 × 3 arrangement of vacancies in the cobalt layer by which structural elements with three- and fourfold coordinated oxygen species are formed. In light of the finding that for 1:1 stoichiometry a CoO monolayer in (111) orientation develops with only threefold coordinated oxygen, stoichiometric properties prove to be of extreme importance in ultrathin films as they can influence the oxide's structure substantially.

Acknowledgment

The authors are indebted to Deutsche Forschungsgemeinschaft for financial support.

References

[1] Meiklejohn W H and Bean C P 1956 *Phys. Rev.* **102** 1413
[2] Meiklejohn W H and Bean C P 1957 *Phys. Rev.* **105** 904
[3] Meyer W, Biedermann K, Gubo M, Hammer L and Heinz K 2008 *J. Phys.: Condens. Matter* **20** 304204
[4] Biedermann K, Gubo M, Hammer L and Heinz K 2009 *J. Phys.: Condens. Matter* **21** 185003
[5] Meyer W, Hock D, Biedermann K, Gubo M, Müller S, Hammer L and Heinz K 2008 *Phys. Rev. Lett.* **101** 016103
[6] Meyer W, Biedermann K, Gubo M, Hammer L and Heinz K 2009 *Phys. Rev.* B **79** 121403(R)
[7] Ignatiev A, Jones A and Rhodin T 1972 *Surf. Sci.* **30** 573
[8] Schmidt A, Meier W, Hammer L and Heinz K 2002 *J. Phys.: Condens. Matter* **14** 12353
[9] Küppers J and Michel H 1979 *Appl. Surf. Sci.* **3** 179
[10] Heinz K, Schmidt G, Hammer L and Müller K 1985 *Phys. Rev.* B **32** 6214
[11] Lerch D, Klein A, Schmidt A, Müller S, Hammer L, Heinz K and Weinert M 2006 *Phys. Rev.* B **73** 075430
[12] Horcas I, Fernandez R, Gomez-Rodriguez J M, Colchero J, Gomez-Herrero J and Baro A M 2007 *Rev. Sci. Instrum.* **78** 013705
[13] Heinz K 1995 *Rep. Prog. Phys.* **58** 637
[14] Rous P J, Pendry J B, Saldin D K, Heinz K, Müller K and Bickel N 1986 *Phys. Rev. Lett.* **57** 2951
[15] Rous P J and Pendry J B 1992 *Prog. Surf. Sci.* **39** 3
[16] Blum V and Heinz K 2001 *Comput. Phys. Commun.* **134** 392
[17] Kottcke M and Heinz K 1997 *Surf. Sci.* **376** 352

[18] Pendry J B 1980 *J. Phys. C: Solid State Phys.* **13** 937
[19] Rundgren J 2003 *Phys. Rev.* B **68** 125405
[20] Baudoing R, Gauthier Y, Lundberg M and Rundgren J 1986 *J. Phys. C: Solid State Phys.* **19** 2825
[21] Döll R, Kottcke M and Heinz K 1993 *Phys. Rev.* B **48** 1973
[22] Heinz K, Kottcke M, Löffler U and Döll R 1996 *Surf. Sci.* **357/358** 1
[23] Giovanardi C, Hammer L and Heinz K 2006 *Phys. Rev.* B **74** 125429
[24] Meyer W 2009 *PhD Thesis* Universität Erlangen-Nürnberg